Enhanced target normal sheath acceleration of protons using multiple laser pulses

J. Ferri[1], E. Siminos[2] and T. Fülöp[1]

[1] *Department of Physics, Chalmers University of Technology, Göteborg, Sweden*

[2] *Department of Physics, University of Gothenburg, Göteborg, Sweden*

Introduction The use of ultra-intense laser pulses interacting with solid targets to accelerate protons or heavier ion species has been thoroughly studied in the past decades [1]. In particular, the target normal sheath acceleration (TNSA) mechanism has been widely improved through numerous experiments, bringing the field closer to many applications, in medicine, industry or basic science. Some recent works proposed to employ several successive laser pulses to improve the performance of the TNSA scheme [2], in order to induce plasma expansion and improve the pulse absorption. However, this mechanism only works for a narrow range of time delay and energy repartition between the two pulses, and would only produce a quite limited energy enhancement.

In this contribution, we describe a modified TNSA scheme in which we use a laser pulse split in two pulses of equal energy, incident on the thin solid target simultaneously, with different angles of incidence. This leads to a standing wave with an increased value of the peak electric field in front of the target. Based on two-dimensional (2D) simulations with the EPOCH Particle-In-Cell (PIC) code [3], we show that it leads to a substantial enhancement of the hot electron generation process and thus, of the TNSA-produced proton energy and number.

Electromagnetic fields in the two-pulse configuration We shall consider two different configurations: (i) the reference case, with one pulse of intensity I_0 incident on the target with an angle ϕ, and (ii) two pulses of intensity $I_0/2$ incident with angles ϕ and $-\phi$. The pulses are p-polarized and are propagating in the x,y plane, with y the direction along the target surface. If we suppose that the target is a perfect conductor, the electric and magnetic fields in the half-space in front of the target are given by the superposition of the incoming and reflected fields. To understand the physical phenomenon leading to the enhanced hot electron production, one could describe the incoming and reflected fields as an effective multi-pulse configuration in the half-space in front of the target. Letting N be the number of effective pulses, it is enough to consider the simple case of N plane waves, with potential $A_n = A_0\sqrt{N/2}\cos(\omega_0 t - k_0\cos(\phi_n) - k_0\sin(\phi_n))$, with ϕ_n the angle of incidence for the n^{th} pulse and where ω_0 is the laser pulsation and $k_0 = \omega_0/c$ with c the speed of light. Note that $N = 2$ in the

reference case and $N = 4$ in the two-pulse case, with the reflection of the n_{th} pulse being given by an incidence angle of $\pi - \phi_n$. The fields in front of the target E_N and B_N are then given by:

$$E_{x,2} = -2\sin\phi E_0 \sin(t - y\sin\phi)\cos(x\cos\phi), \quad E_{x,4} = 2\sqrt{2}E_0 \sin\phi \cos t \sin(y\sin\phi)\cos(x\cos\phi),$$
$$E_{y,2} = -2\cos\phi E_0 \cos(t - y\sin\phi)\sin(x\cos\phi), \quad E_{y,4} = -2\sqrt{2}E_0 \cos\phi \cos t \cos(y\sin\phi)\sin(x\cos\phi),$$
$$B_{z,2} = 2B_0 \sin(t - y\sin\phi)\cos(x\cos\phi), \quad B_{z,4} = 2\sqrt{2}B_0 \sin t \cos(y\sin\phi)\cos(x\cos\phi).$$

In the two pulses case, the fields form a standing wave in front of the target, in contrast to the reference case in which the fields are drifting along y. The key benefit of the two-pulse scheme is that the field amplitude scales as $\sqrt{N}$, so the peak fields are increased by a factor $\sqrt{2}$ in the two-pulse setup. Another important feature of the fields in the two-pulse case is that the magnetic field is zero at the position of the maxima of the E_x field, in contrast to the reference case. This will be important in the electron acceleration process.

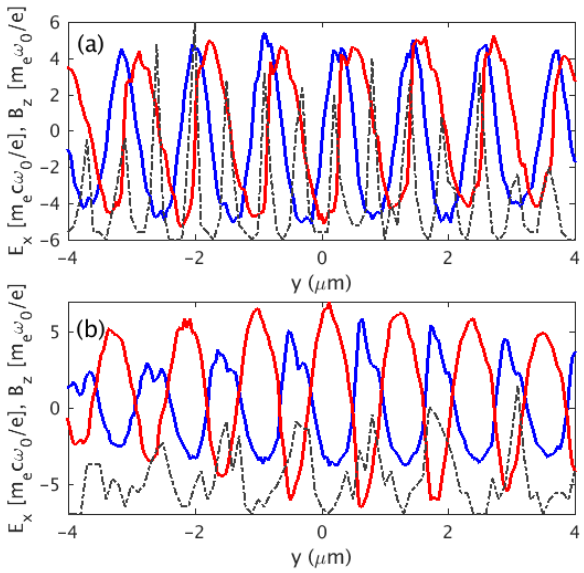

Figure 1: (a) (resp (b)) E_x (blue) and B_z (red) fields on the target surface at $t = 150$ fs in the two-pulse case (resp. reference case). The dashed black line indicate the initial distribution in y on the target surface of the electrons reaching 400 keV. For the reference case, this distribution is plotted in the frame moving with a $c\sin\phi$ velocity along y to take into account the drifting of the fields.

Hot electron generation We now consider the influence of the modification of the fields in front of the target on the hot electron generation in 2D PIC simulations conducted with the EPOCH code. For the reference case, we use a 0.8 J, 38 fs gaussian laser pulse focused on a 5×5 μm^2 spot on a 3 μm-thick, fully-ionized, Aluminum target with a 45° angle of incidence. The target density is 50 n_c for the Al^{13+} ions, with n_c the critical density. For the two-pulse case, the only change is that we instead use two pulses of 0.4 J, with angles $\phi_\pm \pm 45°$. Numerical parameters for these simulations can be found in Ref. [4].

For the same total energy, the modification of the fields in front of the target changes the generation of hot electrons in two ways. First, considering the capacitor model developed by Brunel [5], the average power absorbed per laser cycle P_a for a perfect conductor depends on the incident longitudinal field through: $P_a \propto E_x \left[\left(1 + e^2 E_x^2/m_e^2 c^2 \omega_0^2\right)^{1/2} - 1\right]$, with m_e and e respectively the electron mass and charge. When the incident laser intensity is high enough, P_a is then expected to vary as NE_0^2, to the

benefit of the two-pulse configuration. Note however, that when employing a high number of focused pulses, the field enhancement becomes localized close to the focus. Second, the change in the relative phase between the E_x and the B_z fields also plays a role. In the two-pulse configuration, electrons are pulled out by the eE_x force at the surface of the target. Since these positions correspond to nodes for the B_z field (see Fig. 1(a)), the $v \times B$ force can be neglected. Thus, the electrons simply oscillate due to E_x and can be reinjected in the plasma wih a high momentum. In contrast, in the reference case, $|B_z|$ is also at a maximum when E_x reaches its peak (Fig. 1(b)). As a consequence, the $v \times B$ force cannot be neglected, and it initially opposes the force due to E_x, as soon as the electrons become relativistic, i.e. very rapidly at the intensities considered. The resulting effect is then similar to reducing the initial field E_x felt by the electrons [6].

The hot electron spectra obtained in the two different configurations are plotted in Figure 2, which exhibits a huge increase of the number and energy of the vacuum accelerated electrons in the two-pulse case. We also plot the hot electron spectrum for a case with one pulse containing twice the total energy (1.6 J). The peak value of the field is then the same as in the two-pulse case. However, the temperature of the electron spectra is still inferior to the one obtained in the two-pulse case: this shows the role of the relative phase of the E_x and B_z fields in the two-pulse geometry, where the $v \times B$ force can be neglected.

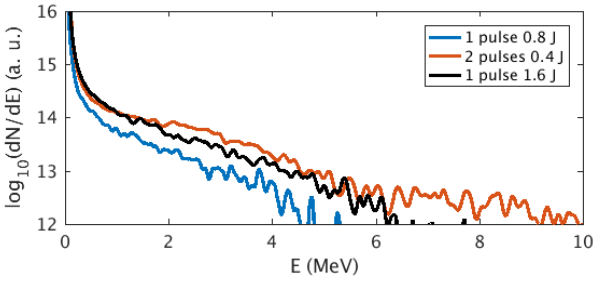

Figure 2: Electron spectra after 160 fs (interaction of the peak of the laser pulse with the target) for the reference case (blue), the two-pulse case (red) and a case with one 1.6 J laser pulse (black).

Proton acceleration The increase of the hot electron energy density in the two-pulse scheme will impact the sheath fields generated on the rear of the target; following the standard estimate yields $E_{x,sheath} \propto \sqrt{n_H, T_H}$, with n_H and T_H the hot electron density and temperature[7]. In turn, this leads to higher proton acceleration for the two-pulse case. Figure 3(a) shows the proton spectra obtained in the simulations with $\phi = 45°$, for protons initially located in a 20 nm-thick layer at the rear of the target in order to model hydrogen-containing impurities. We can see that the maximum proton energy E_{max} increases from 7.8 MeV in the reference case to 13.7 MeV in the two-pulse case (an increase by 80%). Similarly, the number of protons above 1 MeV is multiplied by a factor ~ 5. Note that there is still a $\sim 20\%$ improvement in the maximum proton energy when comparing with the case with a single pulse with twice the energy. Figure 3(b) explores the flexibility of our scheme with respect to the incidence angle.

In the reference case, a clear peak of E_{max} can be observed at 45° as expected from the vacuum heating mechanism. The TNSA mechanism efficiency quickly drops for lower angles, as the $v \times B$ force becomes dominant over the force due to E_x. This is however not happening for the two-pulse case, which can then sustain strong TNSA over a wide range of angles (30°–60°). In experiments it can also be important to have slightly asymmetric angles of incidence for the two pulses, so the reflected pulses are not back-propagating to the optics. Some additional cases are presented in Fig. 3(b), showing that the scheme is largely unaffected with the introduction of a moderate asymmetry (E_{max} is reduced by a mere 7% when using angles $\phi_1 = 35°$, $\phi_2 = -55°$), which opens the way toward experiments.

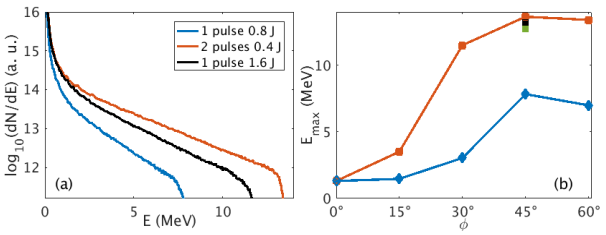

Figure 3: (a) Proton spectra after 700 fs in the reference case (blue), the two-pulse case (red) and a case with one 1.6 J laser pulse (black). (b) Dependence of the maximum proton energy as a function of the incidence angle. For the two-pulse case, the angles are ϕ and $-\phi$. Additionnal squares correspond to asymmetric cases, with $\phi_1 = 40°$, $\phi_2 = -50°$ (black) and $\phi_1 = 35°$ and $\phi_2 = -55°$ (green).

Conclusion We present a scheme consisting in a modification of the TNSA scheme with the aim of enhancing the proton energy and number, for a constant laser energy. In this scheme, two laser pulses are incident simulateneously at different angles on a solid target. This allows for high improvement of the proton energy in realistic conditions, and these results are robust over a large range of angles. Moreover, the performance could even be further improved by exploring configurations involving the splitting of the laser pulse in a larger number of sub-pulses.

References

[1] H. Daido et al., Rep. Prog. Phys. **75**, 056401 (2012); A. Macchi et al., Rev. Mod. Phys. **85**, 751 (2013).

[2] K. Markey et al., Phys. Rev. Lett. **105**, 195008 (2010); C. Brenner et al., App. Phys. Lett. **104**, 081123 (2014); J. Ferri et al., Phys. Plasmas **25**, 043115 (2018).

[3] T. Arber et al., Plasma Phys. Control. Fusion **57**, 1 (2015).

[4] J. Ferri et al., arXiv:1806.04912. (2018)

[5] F. Brunel, Phys. Rev. Lett. **59**, 52 (1987).

[6] J. P. Geindre et al., Phys. Rev. Lett. **97**, 085001 (2006).

[7] P. Mora, Phys. Rev. Lett. **90**, 185002 (2003).